A Constitutive Formulation for Polymers Subjected to High Strain Rates

S. Kolling[1], A. Haufe[2], M. Feucht[1], P.A. Du Bois[3],
[1] *DaimlerChrysler AG, EP/CSB, HPC X411, D-71059 Sindelfingen, Germany*
[2] *Dynamore GmbH, Industriestr. 2, D-70565 Stuttgart, Germany*
[3] *Consulting Engineer, Freiligrathstr. 6, 63071 Offenbach, Germany*

Abstract

Reliable prediction of the behavior of structures made from polymers is a topic under considerable investigation in engineering practice. Especially, if the structure is subjected to dynamic loading, constitutive models considering the mechanical behavior properly are still not available in commercial finite element codes yet. In our paper, we present a new constitutive law for polymers which recovers important phenomena like necking, crazing, strain rate dependency, unloading behavior and damage. In particular, different yield surfaces in compression and tension and strain rate dependent failure, the latter with damage induced erosion, is taken into account. All relevant parameters are given directly in the input as load curves, i.e. time consuming parameter identification is not necessary. Moreover, the models by von Mises and Drucker-Prager are included in the description as special cases.
With the present formulation, standard verification test can be simulated successfully: tensile and compression test, shear test and three point bending tests.

1. Introduction

Under high velocity impact loading, thermoplastic components undergo large plastic deformations and will most likely fail. Consequently, the unloading behavior is irrelevant and thermoplastics can be modeled with a sufficiently good approximation as pseudo-metallic elastic-plastic bodies. This is, however, not always the case – even in crashworthiness applications. Nowadays important applications in crash simulation that demand a more accurate modeling of thermoplastics are simulation problems in pedestrian protection, e.g. head and leg impact (see [4], [7], [8]) and passenger protection. Although highly sophisticated material laws are available in commercial finite element programs, there are still open questions, especially in the aforementioned field of application. In this paper, the main focus is set to the explicit solver of LS-DYNA [1], [2] but clearly with some effort all results are transferable to other solvers. In the following, an overview on classical models for polymers which are used for crash simulations nowadays is given. From a practical point of view, the usually applied constitutive model is material no. 24, a classical elastic-plastic model based on the von Mises criteria. It should be strongly emphasized though, that thermoplastics are not incompressible during plastic flow. This leads to the conclusion that material laws based on the von Mises criterion are not suitable in general [9], [10]. Therefore, a new material model which has been implemented into LS-DYNA as a user defined constitutive model will be the main focus of the present contribution. A new constitutive model, termed as SAMP-1 (**S**emi-**A**nalytical **M**odel for **P**olymers with C^1-differentiable yield surface, see [3]) is derived in the following. The main focus of the present project is to include all relevant experimentally observed effects in one model.

2. Material Law Formulation

2.1. Yield surface formulation for plastics

2.1.1. Choice of a yield surface formulation

All plastics are to some degree anisotropic. The anisotropic characteristic can be due to fiber reinforcement, to the molding process or it can be load induced in which case the material is at least initially isotropic. Therefore a quadratic form in the stress tensor is often used to describe the yield surface (see Bardenheier [5]). We restrict the scope of this work to isotropic formulations. However, the choice of this yield surface was made in view of later anisotropic generalizations. In the isotropic case the most general quadratic yield surface can be written as

$$f = \boldsymbol{\sigma}^{\mathrm{T}}\mathbf{F}\boldsymbol{\sigma} + \mathbf{B}\boldsymbol{\sigma} + F_0 \le 0, \text{ where} \tag{1}$$

$$\boldsymbol{\sigma} = \begin{pmatrix} \sigma_{xx} \\ \sigma_{yy} \\ \sigma_{zz} \\ \sigma_{xy} \\ \sigma_{yz} \\ \sigma_{zx} \end{pmatrix} \quad \mathbf{F} = \begin{pmatrix} F_{11} & F_{12} & F_{12} & 0 & 0 & 0 \\ F_{12} & F_{11} & F_{12} & 0 & 0 & 0 \\ F_{12} & F_{12} & F_{11} & 0 & 0 & 0 \\ 0 & 0 & 0 & F_{44} & 0 & 0 \\ 0 & 0 & 0 & 0 & F_{44} & 0 \\ 0 & 0 & 0 & 0 & 0 & F_{44} \end{pmatrix} \quad \mathbf{B} = \begin{pmatrix} F_1 & 0 & 0 & 0 & 0 & 0 \\ 0 & F_1 & 0 & 0 & 0 & 0 \\ 0 & 0 & F_1 & 0 & 0 & 0 \\ 0 & 0 & 0 & 0 & 0 & 0 \\ 0 & 0 & 0 & 0 & 0 & 0 \\ 0 & 0 & 0 & 0 & 0 & 0 \end{pmatrix}. \tag{2}$$

Some restrictions apply to the choice of the coefficients (see [14]). The existence of a stress-free state and the equivalence of pure shear and biaxial tension/compression require respectively $F_0 \le 0$ *and* $F_{44} = 2(F_{11} - F_{12})$. Although four independent coefficients remain in the expression for the isotropic yield surface at this point, the yield condition is not affected if all coefficients are multiplied by a constant. Consequently only three coefficients can be freely chosen and three experiments under different states of stress can be fitted by this formulation. Without loss of generality the expression for the yield surface can be reformulated in terms of the first two stress invariants: pressure and von Mises stress.

$$\begin{aligned} p &= -\frac{\sigma_{xx} + \sigma_{yy} + \sigma_{zz}}{3} \\ \sigma_{vm} &= \sqrt{\frac{3}{2}\left((\sigma_{xx} + p)^2 + (\sigma_{yy} + p)^2 + (\sigma_{zz} + p)^2 + 2\sigma_{xy}^2 + 2\sigma_{yz}^2 + 2\sigma_{zx}^2\right)} \end{aligned} \tag{3}$$

The expression for the yield surface then becomes $f = \sigma_{vm}^2 - A_0 - A_1 p - A_2 p^2 \le 0$. and identification of the coefficients leads to $A_0 = -F_0$, $A_1 = 3F_1$ *and* $A_2 = 9(1 - F_{11})$ or equivalently

$$F_0 = -A_0,\ F_1 = \frac{A_1}{3},\ F_{11} = 1 - \frac{A_2}{9},\ F_{44} = 3 \ \textit{and} \ F_{12} = F_{11} - \frac{F_{44}}{2} = -\left(\frac{1}{2} + \frac{A_2}{9}\right). \tag{4}$$

Since there is no loss of generality, the simpler formulation in invariants is adopted from this point on. In principle the coefficients of the yield surface can now be determined from the aforementioned three experiments. Typically one would perform uniaxial tension, uniaxial compression and simple shear tests. This allows computation of the coefficients as functions of the test results:

$$\left.\begin{array}{c} 3\sigma_s^2 = A_0 \\ \sigma_t^2 = 3\sigma_s^2 - A_1\dfrac{\sigma_t}{3} + A_2\dfrac{\sigma_t^2}{9} \\ \sigma_c^2 = 3\sigma_s^2 + A_1\dfrac{\sigma_c}{3} + A_2\dfrac{\sigma_c^2}{9} \end{array}\right\} \Rightarrow \left\{\begin{array}{c} A_0 = 3\sigma_s^2 \\ A_1 = 9\sigma_s^2\left(\dfrac{\sigma_c - \sigma_t}{\sigma_c\sigma_t}\right) \\ A_2 = 9\left(\dfrac{\sigma_c\sigma_t - 3\sigma_s^2}{\sigma_c\sigma_t}\right) \end{array}\right. \tag{5}$$

Alternatively one may also compute the coefficients relating to the formulation in stress space:

$$\left.\begin{array}{c} F_0 + F_1\sigma_t + F_{11}\sigma_t^2 = 0 \\ F_0 - F_1\sigma_c + F_{11}\sigma_c^2 = 0 \\ F_0 + F_{44}\sigma_s^2 = 0 \end{array}\right\} \Rightarrow \left\{\begin{array}{c} F_1 = F_0\left(\dfrac{1}{\sigma_c} - \dfrac{1}{\sigma_t}\right) \\ F_{11} = -\dfrac{F_0}{\sigma_t\sigma_c} \\ F_{44} = -\dfrac{F_0}{\sigma_s^2} \end{array}\right. \tag{6}$$

2.1.2. Conditions for convexity of the yield surface

Introductory remarks

Usually the yield surface is required to be convex, i.e.

$$\left.\begin{array}{l} f(\boldsymbol{\sigma}_1) \le 0 \\ f(\boldsymbol{\sigma}_2) \le 0 \\ 0 \le \alpha \le 1 \end{array}\right\} \Rightarrow\ f(\alpha\boldsymbol{\sigma}_1 + (1-\alpha)\boldsymbol{\sigma}_2) \le 0 \tag{7}$$

The second derivative of *f* is computed as $f = \boldsymbol{\sigma}^{\mathrm{T}}\mathbf{F}\boldsymbol{\sigma} + \mathbf{B}\boldsymbol{\sigma} + F_0 \ \rightarrow\ \dfrac{\partial^2 f}{\partial\sigma^2} = 2\mathbf{F}$. A sufficient condition for convexity in 6D stress space is then that the matrix **F** should be positive semidefinite. This means all eigenvalues of **F** should be positive or zero. The conditions for convexity will now be examined in physical terms for two cases: plane stress and general 3D.

The plane stress case

In the plane stress case the yield condition reduces to:

$$f = \boldsymbol{\sigma}^{\mathbf{T}}\mathbf{F}\boldsymbol{\sigma} + \mathbf{B}\boldsymbol{\sigma} + F_0 \tag{8}$$

where

$$\boldsymbol{\sigma} = \begin{pmatrix} \sigma_{xx} \\ \sigma_{yy} \\ \sigma_{xy} \end{pmatrix} \quad \mathbf{F} = \begin{pmatrix} F_{11} & F_{12} & 0 \\ F_{12} & F_{11} & 0 \\ 0 & 0 & F_{44} \end{pmatrix} \quad \mathbf{B} = \begin{pmatrix} F_1 & 0 & 0 \\ 0 & F_1 & 0 \\ 0 & & 0 \end{pmatrix}. \tag{9}$$

Furthermore convexity requires the eigenvalues of **F** to be non-negative:

$$\left.\begin{array}{c} F_{11}+F_{12}\geq 0 \\ F_{11}-F_{12}\geq 0 \\ F_{44}\geq 0 \end{array}\right\} \Rightarrow \begin{cases} 4\sigma_s^2 \geq \sigma_t\sigma_c \\ -F_0 \geq 0 \end{cases} \tag{10}$$

Representation of the yield surface in the principal stress space allows a geometrical interpretation. Clearly as long as $\sigma_s > \sqrt{\sigma_t\sigma_c}/2$, the yield surface is elliptic and thus convex. In the case of $\sigma_s = \sqrt{\sigma_t\sigma_c}/2$ the yield surface degenerates into two straight lines. And for $\sigma_s < \sqrt{\sigma_t\sigma_c}/2$ the yield surface becomes hyperbolic and convexity is lost. A non-convex yield surface is physically not plausible under plane stress conditions since no yielding would occur under biaxial loading.
In the invariant plane the convexity condition for the plane stress case is easily seen to lead to the following condition:

$$\sigma_S \geq \frac{\sqrt{\sigma_t\sigma_c}}{2''} \Rightarrow A_2 \leq \frac{9}{4} \tag{11}$$

Thus, positive values of A_2 are allowed and the yield curve can actually show a limited positive curvature. Convex yield surfaces in principal stress space are guaranteed as long as the yield curve has a finite intersection with the biaxial line, .i.e.

$$\left.\begin{array}{c} \sigma_{vm}^2 - A_0 - A_1 p - A_2 p^2 = 0 \\ \sigma_{vm} = \pm\frac{3p}{2} \end{array}\right\} \frac{9p^2}{4} - A_0 - A_1 p - A_2 p^2 = 0\,. \tag{12}$$

This last equation will have a real finite solution for the pressure p iff

$$A_1^2 + 4A_0\left(\frac{9}{4} - A_2\right) \geq 0 \Rightarrow \sigma_s \geq \frac{\sqrt{\sigma_t\sigma_c}}{2}, \tag{13}$$

which is equivalent to requiring a convex yield surface in principal stress space.

The 3D case

In the full 3D case, the convexity condition is generally more stringent. Again we require the eigenvalues of **F** to be non-negative, where **F** is now the full 6 by 6 matrix:

$$\left.\begin{array}{c} F_{11}+2F_{12}\geq 0 \\ F_{11}-F_{12}\geq 0 \\ F_{44}\geq 0 \end{array}\right\} \Rightarrow \begin{cases} 3\sigma_s^2 \geq \sigma_t\sigma_c \\ -F_0 \geq 0 \end{cases} \text{ leading to } \sigma_s \geq \frac{\sqrt{\sigma_t\sigma_c}}{\sqrt{3}} > \frac{\sqrt{\sigma_t\sigma_c}}{2}.$$

Note that the trivial conditions $\sigma_s \geq 0,\ \sigma_c \geq 0,\ \sigma_t \geq 0,\ F_0 \leq 0$ are already sufficient to ensure $F_{44} \geq 0,\ F_{11} \geq 0,\ F_{11} - F_{12} = 2F_{44} \geq 0$ .And consequently, only the first eigenvalue may be negative. Note that the condition that the first eigenvalue must not be negative can be reformulated as $F_{11} + 2F_{12} = -\frac{A_2}{9} \geq 0 \Rightarrow A_2 \leq 0$. In 3D principal stress space a convex quadratic yield surface corresponds to an ellipsoid, a cylinder or an ellipsoidal paraboloid. It should be noted here, that convexity in stress space is a sufficient condition for convexity in the invariant space spanned by the

pressure and the von Mises stress but the reverse is not the case. Indeed consider the case of a linear relationship between the invariants (Drucker-Prager type law). This is a limiting case for convexity in the invariant plane and

$$\sqrt{3}\sigma_s = \frac{2\sigma_t\sigma_c}{\sigma_t+\sigma_c} \Rightarrow \sigma_s = \frac{\sqrt{\sigma_t\sigma_c}}{\sqrt{3}}\frac{2\sqrt{\sigma_t\sigma_c}}{\sigma_t+\sigma_c} \le \frac{\sqrt{\sigma_t\sigma_c}}{\sqrt{3}} \quad . \tag{14}$$

Thus it is shown that this yield surface is not convex in stress space if $\sigma_c = \sigma_t$. This corresponds to the von Mises cylinder. In general, a Drucker-Prager type law is represented by a cone in principal stress space. This surface is strictly spoken not convex because the cone consists of two blades. To complete our discussion a formal derivation of the convexity condition in the invariant plane is given by

$$f = \sigma_{vm}^2 - A_0 - A_1 p - A_2 p^2, \sigma_{vm} = \sqrt{A_0 + A_1 p + A_2 p^2}, \frac{\partial^2 \sigma_{vm}}{\partial p^2} \le 0 \Rightarrow \sigma_s \ge \frac{2\sigma_t\sigma_c}{\sqrt{3}(\sigma_t+\sigma_c)} \tag{15}$$

2.2. Flow rule

Associated flow leads to the plastic strain rate in terms of the normal vector to the yield surface

$$\dot{\boldsymbol{\varepsilon}}_{\mathbf{p}} = \dot{\lambda}\mathbf{n} = \dot{\lambda}\frac{\dfrac{\partial f}{\partial \boldsymbol{\sigma}}}{\left\|\dfrac{\partial f}{\partial \boldsymbol{\sigma}}\right\|} \qquad \left\|\frac{\partial f}{\partial \boldsymbol{\sigma}}\right\| = \sqrt{\frac{\partial f}{\partial \boldsymbol{\sigma}} : \frac{\partial f}{\partial \boldsymbol{\sigma}}} \quad . \tag{16}$$

The volumetric plastic strain rate, deviatoric plastic strain rate and equivalent plastic strain rate are defined in the usual way:

$$\dot{\varepsilon}_{pv} = tr\left(\dot{\boldsymbol{\varepsilon}}_{\mathbf{p}}\right) = \frac{\dot{\lambda}}{\left\|\dfrac{\partial f}{\partial \boldsymbol{\sigma}}\right\|} tr\left(\frac{\partial f}{\partial \boldsymbol{\sigma}}\right),\ \dot{\varepsilon}_{\mathrm{pd}} = \dot{\varepsilon}_{\mathrm{p}} - \frac{\dot{\varepsilon}_{pv}}{3}\delta,\ \dot{\varepsilon}_p = \sqrt{\frac{2}{3}\dot{\varepsilon}_{\mathrm{pd}} : \dot{\varepsilon}_{\mathrm{pd}}} = \frac{\dot{\lambda}}{\left\|\dfrac{\partial f}{\partial \sigma}\right\|}\sqrt{\frac{2}{3}\left.\frac{\partial f}{\partial \sigma}\right|_{\mathrm{d}} : \left.\frac{\partial f}{\partial \sigma}\right|_{\mathrm{d}}} \tag{17}$$

The associated flow for the general quadratic yield surface is defined as

$$\left.\begin{array}{l} \dfrac{\partial \sigma_{vm}}{\partial \sigma} = \dfrac{3}{2\sigma_{vm}}\mathrm{s} \\ \dfrac{\partial p}{\partial \sigma} = -\dfrac{1}{3}\delta \end{array}\right\} \Rightarrow \frac{\partial f}{\partial \sigma} = 3\mathrm{s} + \frac{A_1 + 2A_2 p}{3}\delta,\ \left\|\frac{\partial f}{\partial \sigma}\right\| = \sqrt{6\sigma_{vm}^2 + \frac{1}{3}(A_1 + 2A_2 p)^2} \tag{18}$$

leading to the volumetric and deviatoric plastic strain rates respectively:

$$\dot{\varepsilon}_{vp} = \dot{\lambda}(A_1 + 2A_2 p)\Big/\left\|\frac{\partial f}{\partial \sigma}\right\|,\ \dot{\varepsilon}_{\mathrm{dp}} = \dot{\lambda}3\mathrm{s}\Big/\left\|\frac{\partial f}{\partial \sigma}\right\| \tag{19}$$

The equivalent plastic strain rate reads:

$$\dot{\varepsilon}_p = \sqrt{\frac{2}{3}\dot{\varepsilon}_{\mathrm{dp}} : \dot{\varepsilon}_{\mathrm{dp}}} = \dot{\lambda}\sqrt{\frac{2}{3}3\mathrm{s} : 3\mathrm{s}}\Big/\left\|\frac{\partial f}{\partial \sigma}\right\|,\ \dot{\varepsilon}_p = \dot{\lambda}2\sigma_{vm}\Big/\left\|\frac{\partial f}{\partial \sigma}\right\| \tag{20}$$

It is instructive to derive the ratio of transversal to longitudinal plastic strain rate under uniaxial tensile and compressive loading. This ratio will here be called the *"plastic Poisson ratio"* although of course it is by no means a material constant:

$$\nu_p = -\frac{\dot{\varepsilon}_{yyp}}{\dot{\varepsilon}_{xxp}} = -\frac{\dot{\varepsilon}_{zzp}}{\dot{\varepsilon}_{xxp}} \tag{21}$$

It will be shown that additional restrictions are placed on the shape of the yield surface in order for the lateral behavior of the material model to be reasonable under plastic loading. We therefore compute the plastic Poisson ratio in function of the yield surface:

$$\left.\begin{aligned} \dot{\varepsilon}_{vp} &= (1-2\nu_p)\dot{\varepsilon}_{xxp} \\ \dot{\varepsilon}_{xxp} &= \dot{\lambda}\left(3s_{xx} + \frac{A_1 + 2A_2 p}{3}\right)/\|\mathbf{n}\| \\ \dot{\varepsilon}_{vp} &= \dot{\lambda}(A_1 + 2A_2 p)/\|\mathbf{n}\| \\ s_{xx} &= -2p \end{aligned}\right\} \Rightarrow A_1 + 2A_2 p = (1-2\nu_p)\left(-6p + \frac{A_1 + 2A_2 p}{3}\right) \tag{22}$$

This last expression yields $\nu_p = \dfrac{9 + 2A_2 + A_1/p}{18 - 2A_2 - A_1/p}$ and shows that the plastic Poisson ratio is dependent on the pressure and in particular that the lateral behavior of the material is different in tension and in compression. This can be estimated further as:

$$\begin{cases} p < 0 \Rightarrow p = -\dfrac{\sigma_t}{3} \Rightarrow \nu_p = \dfrac{9 + 2A_2 - 3A_1/\sigma_t}{18 - 2A_2 + 3A_1/\sigma_t} = \dfrac{\sigma_t^2}{\sigma_s^2}\dfrac{\sigma_c}{\sigma_t + \sigma_c} - 1 \\ p > 0 \Rightarrow p = \dfrac{\sigma_c}{3} \Rightarrow \nu_p = \dfrac{9 + 2A_2 + 3A_1/\sigma_c}{18 - 2A_2 - 3A_1/\sigma_c} = \dfrac{\sigma_c^2}{\sigma_s^2}\dfrac{\sigma_t}{\sigma_t + \sigma_c} - 1 \end{cases} \tag{23}$$

These equations can be solved for the shear yield:

$$\begin{cases} p < 0 \Rightarrow \nu_p = \dfrac{\sigma_t^2}{\sigma_s^2}\dfrac{\sigma_c}{\sigma_t + \sigma_c} - 1 \Rightarrow \sigma_s^2 = \dfrac{\sigma_t^2}{1+\nu_p}\dfrac{\sigma_c}{\sigma_t + \sigma_c} \\ p > 0 \Rightarrow \nu_p = \dfrac{\sigma_c^2}{\sigma_s^2}\dfrac{\sigma_t}{\sigma_t + \sigma_c} - 1 \Rightarrow \sigma_s^2 = \dfrac{\sigma_c^2}{1+\nu_p}\dfrac{\sigma_t}{\sigma_t + \sigma_c} \end{cases} \tag{24}$$

The latter shows that reasonable values for the plastic Poisson ratio put certain requirements on the yield surface:

$$0 \ge \nu_p \ge 0.5 \Rightarrow \begin{cases} p < 0 \Rightarrow \dfrac{\sigma_t\sigma_c}{3}\dfrac{2\sigma_t}{\sigma_t + \sigma_c} \le \sigma_s^2 \le \dfrac{\sigma_t\sigma_c}{3}\dfrac{3\sigma_t}{\sigma_t + \sigma_c} \\ p > 0 \Rightarrow \dfrac{\sigma_t\sigma_c}{3}\dfrac{2\sigma_c}{\sigma_t + \sigma_c} \le \sigma_s^2 \le \dfrac{\sigma_t\sigma_c}{3}\dfrac{3\sigma_c}{\sigma_t + \sigma_c} \end{cases} \tag{25}$$

Whereas convexity required only a lower limit for the shear yield, plausible plastic flow also imposes an upper limit with respect to tensile and compressive yield values. As it will be difficult in general to guarantee reasonable flow behavior from three independent measurements in

shear, tension and compression, a simplified flow rule has been implemented as the default in SAMP-1. The generally non-associated flow surface is given as

$$g = \sigma_{vm}^2 + \alpha p^2 . \tag{26}$$

This flow rule is associated iff $A_1 = 0, \quad A_2 = -\alpha$. And clearly leads to a constant value for the plastic Poisson ratio if α is a constant

$$\nu_p = \frac{9-2\alpha}{18+2\alpha} \Rightarrow \alpha = \frac{9}{2}\frac{1-2\nu_p}{1+\nu_p} . \tag{27}$$

Plausible flow behavior just means that $0 \le \alpha \le \frac{9}{2} \Rightarrow 0 \le \nu_p \le 0.5$. In SAMP-1 the value of the plastic Poisson coefficient is given by the user, either as a constant or as a load curve in function of the uniaxial plastic strain. This allows to adjust the flow rule of the material to measurements of transversal deformation during uniaxial tensile or compressive testing. This can be important for plastics since often a non-isochoric behavior is measured.

The volumetric and deviatoric plastic strain rates in this case are given as

$$\dot{\varepsilon}_{vp} = \dot{\lambda}(-2\alpha p)\Big/\left\|\frac{\partial g}{\partial \sigma}\right\| = \frac{\dot{\lambda}(-2\alpha p)}{\sqrt{6\sigma_{\mathrm{vm}}^2 + \frac{4}{3}\alpha^2 p^2}}, \; \dot{\varepsilon}_{\mathrm{dp}} = \dot{\lambda}3\mathrm{s}\Big/\left\|\frac{\partial g}{\partial \sigma}\right\| = \frac{\dot{\lambda}3\mathrm{s}}{\sqrt{6\sigma_{\mathrm{vm}}^2 + \frac{4}{3}\alpha^2 p^2}} \quad . \tag{28}$$

In SAMP-1 the formulation is slightly modified and based on a flow rule $g' = \sqrt{\sigma_{vm}^2 + \alpha p^2}$.

The plastic strain rate computation is not normalized: $\dot{\boldsymbol{\varepsilon}}_{\mathbf{p}} = \dot{\lambda}\frac{\partial g'}{\partial \boldsymbol{\sigma}}$. The volumetric and deviatoric plastic strain rates in this case are given as:

$$\begin{aligned} \dot{\varepsilon}_{vp} &= \dot{\lambda}(-2\alpha p)\big/2g' = \frac{\dot{\lambda}(-2\alpha p)}{\sqrt{4\sigma_{\mathrm{vm}}^2 + 4\alpha p^2}} \\ \dot{\varepsilon}_{\mathrm{dp}} &= \dot{\lambda}3\mathrm{s}\big/2g' = \frac{\dot{\lambda}3\mathrm{s}}{\sqrt{4\sigma_{\mathrm{vm}}^2 + 4\alpha p^2}} \end{aligned} \tag{29}$$

This amounts to a different definition of the plastic consistency parameter $\dot{\lambda}$ which of course has to be considered when equivalent plastic strain values are computed.

2.3. Hardening formulation

The hardening formulation is the attractive part of SAMP-1. The formulation is fully tabulated and consequently the user can directly input measurement results from uniaxial tension, uniaxial compression and simple shear tests in terms of load curves giving the yield stress as a function of the corresponding plastic strain. No fitting of coefficients is required. The test results that are reflected in the load curves will be used exactly by SAMP-1 without fitting to any analytical expression. Consequently the hardening will be dependent on the state of stress and not only on the

plastic strain. The hardening rule now requires to define the evolution of all hardening parameters as a function of the plastic consistency parameter:

$$\dot{A}_0 = \frac{\partial A_0}{\partial \lambda}\dot{\lambda},\ \dot{A}_1 = \frac{\partial A_1}{\partial \lambda}\dot{\lambda},\ \dot{A}_2 = \frac{\partial A_2}{\partial \lambda}\dot{\lambda},\ \dot{\alpha} = \frac{\partial \alpha}{\partial \lambda}\dot{\lambda}. \tag{30}$$

The first three equations must be rewritten as follows:

$$\left.\begin{array}{c} A_0 = 3\sigma_s^2 \\ \dfrac{\partial A_0}{\partial \lambda} = \dfrac{\partial A_0}{\partial \sigma_s}\dfrac{\partial \sigma_s}{\partial \lambda} + \dfrac{\partial A_0}{\partial \sigma_t}\dfrac{\partial \sigma_t}{\partial \lambda} + \dfrac{\partial A_0}{\partial \sigma_c}\dfrac{\partial \sigma_c}{\partial \lambda} \end{array}\right\} \frac{\partial A_0}{\partial \lambda} = 6\sigma_s\frac{\partial \sigma_s}{\partial \lambda} \tag{31}$$

$$\left.\begin{array}{c} A_1 = 9\sigma_s^2\dfrac{\sigma_c - \sigma_t}{\sigma_t\sigma_c} \\ \dfrac{\partial A_1}{\partial \lambda} = \dfrac{\partial A_1}{\partial \sigma_s}\dfrac{\partial \sigma_s}{\partial \lambda} + \dfrac{\partial A_1}{\partial \sigma_t}\dfrac{\partial \sigma_t}{\partial \lambda} + \dfrac{\partial A_1}{\partial \sigma_c}\dfrac{\partial \sigma_c}{\partial \lambda} \end{array}\right\} \frac{\partial A_1}{\partial \lambda} = 18\sigma_s\frac{\sigma_c - \sigma_t}{\sigma_t\sigma_c}\frac{\partial \sigma_s}{\partial \lambda} - 9\frac{\sigma_s^2}{\sigma_t^2}\frac{\partial \sigma_t}{\partial \lambda} + 9\frac{\sigma_s^2}{\sigma_c^2}\frac{\partial \sigma_c}{\partial \lambda} \tag{32}$$

$$\left.\begin{array}{c} A_2 = 9\left(\dfrac{\sigma_t\sigma_c - 3\sigma_s^2}{\sigma_t\sigma_c}\right) \\ \dfrac{\partial A_2}{\partial \lambda} = \dfrac{\partial A_2}{\partial \sigma_s}\dfrac{\partial \sigma_s}{\partial \lambda} + \dfrac{\partial A_2}{\partial \sigma_t}\dfrac{\partial \sigma_t}{\partial \lambda} + \dfrac{\partial A_2}{\partial \sigma_c}\dfrac{\partial \sigma_c}{\partial \lambda} \end{array}\right\} \frac{\partial A_2}{\partial \lambda} = 9\left(-\frac{6\sigma_s}{\sigma_t\sigma_c}\frac{\partial \sigma_s}{\partial \lambda} + \left(\frac{3\sigma_s^2}{\sigma_t^2\sigma_c}\right)\frac{\partial \sigma_t}{\partial \lambda} + \left(\frac{3\sigma_s^2}{\sigma_t\sigma_c^2}\right)\frac{\partial \sigma_c}{\partial \lambda}\right) \tag{33}$$

The following conversion

$$\frac{\partial \sigma_s}{\partial \lambda} = \frac{\partial \sigma_s}{\partial \varepsilon_{ps}}\frac{\partial \varepsilon_{ps}}{\partial \lambda},\quad \frac{\partial \sigma_t}{\partial \lambda} = \frac{\partial \sigma_t}{\partial \varepsilon_{pt}}\frac{\partial \varepsilon_{pt}}{\partial \lambda},\quad \frac{\partial \sigma_c}{\partial \lambda} = \frac{\partial \sigma_c}{\partial \varepsilon_{pc}}\frac{\partial \varepsilon_{pc}}{\partial \lambda} \tag{34}$$

is defined to fully determine the hardening mechanism by performing three table lookups during every iteration in each time step. The table lookups give the yield stress and the tangent as a function of plastic strain for each experiment. From λ we obtain:

$$\varepsilon_{ps} \Rightarrow \sigma_s, \frac{\partial \sigma_s}{\partial \varepsilon_{ps}},\quad \varepsilon_{pt} \Rightarrow \sigma_t, \frac{\partial \sigma_t}{\partial \varepsilon_{pt}},\quad \varepsilon_{pc} \Rightarrow \sigma_c, \frac{\partial \sigma_c}{\partial \varepsilon_{pc}} \tag{35}$$

What remains to be done is to establish the relationship between the plastic consistency parameter and the plastic strains that were measured under uniaxial tension/compression and simple shear. To achieve this, the equivalent plastic strain rate as a function of the plastic consistency parameter is generally used. Note that the hardening rule must be carefully considered at this point. Furthermore, the relationship between the individual plastic strain rate values and the consistency parameter is established. For the uniaxial case we get

$$\dot{\varepsilon}_p = \begin{pmatrix} \dot{\varepsilon}_{pct} & 0 & 0 \\ 0 & -\nu_p\dot{\varepsilon}_{pct} & 0 \\ 0 & 0 & -\nu_p\dot{\varepsilon}_{pct} \end{pmatrix},\ \dot{\varepsilon}_p = \left|\dot{\varepsilon}_{pct}\right|\frac{2}{3}\left(1+\nu_p\right),\ \left|\dot{\varepsilon}_{pct}\right| = \begin{cases} \dot{\lambda}\dfrac{\sigma_{vm}}{g}\dfrac{3}{2\left(1+\nu_p\right)} \\ \dot{\lambda}\dfrac{2\sigma_{vm}}{\|\mathrm{n}\|}\dfrac{3}{2\left(1+\nu_p\right)} \end{cases}. \tag{36}$$

Similarly the plastic strain rate under shear loading is obtained by

$$\dot{\varepsilon}_{\mathrm{p}} = \dot{\varepsilon}_{\mathrm{dp}} = \begin{pmatrix} 0 & \dot{\varepsilon}_{ps} & 0 \\ \dot{\varepsilon}_{ps} & 0 & 0 \\ 0 & 0 & 0 \end{pmatrix}, \dot{\varepsilon}_p = \frac{2}{\sqrt{3}}\left|\dot{\varepsilon}_{ps}\right|, \left|\dot{\varepsilon}_{ps}\right| = \begin{cases} \dot{\lambda}\dfrac{\sigma_{vm}}{g}\dfrac{\sqrt{3}}{2} = \dot{\lambda}\dfrac{\sqrt{3}}{2} \\ \dot{\lambda}\dfrac{2\sigma_{vm}}{\|\mathrm{n}\|}\dfrac{\sqrt{3}}{2} \end{cases} . \tag{37}$$

These equations always allow determination of individual plastic strain values and thus the abscissa values for the table-lookup operations from the plastic consistency parameter.

$$\left|\dot{\varepsilon}_{pct}\right| = \dot{\varepsilon}_p \frac{3}{2(1+\nu_p)} = \begin{cases} \dot{\lambda}\dfrac{\sigma_{vm}}{g}\dfrac{3}{2(1+\nu_p)} \Rightarrow \left|\varepsilon_{pct}\right| = \displaystyle\int \frac{\sigma_{vm}}{g}\frac{3}{2(1+\nu_p)}d\lambda \\ \dot{\lambda}\dfrac{2\sigma_{vm}}{\|\mathbf{n}\|}\dfrac{3}{2(1+\nu_p)} \Rightarrow \left|\varepsilon_{pct}\right| = \displaystyle\int \frac{\sigma_{vm}}{\|\mathbf{n}\|}\frac{3}{(1+\nu_p)}d\lambda \end{cases} \tag{38}$$

$$\left|\dot{\varepsilon}_{ps}\right| = \dot{\varepsilon}_p \frac{\sqrt{3}}{2} = \begin{cases} \dot{\lambda}\dfrac{\sigma_{vm}}{g}\dfrac{\sqrt{3}}{2} = \dot{\lambda}\dfrac{\sqrt{3}}{2} \Rightarrow \left|\varepsilon_{ps}\right| = \lambda\dfrac{\sqrt{3}}{2} \\ \dot{\lambda}\dfrac{2\sigma_{vm}}{\|\mathbf{n}\|}\dfrac{\sqrt{3}}{2} \Rightarrow \left|\varepsilon_{ps}\right| = \displaystyle\int \frac{2\sigma_{vm}}{\|\mathbf{n}\|}\frac{\sqrt{3}}{2}d\lambda \end{cases} \tag{39}$$

In case of non-associated flow and a constant plastic Poisson ratio the integration is easily done analytically:

$$\left|\dot{\varepsilon}_{pct}\right| = \dot{\lambda}\frac{\sigma_{vm}}{g}\frac{3}{2(1+\nu_p)} \quad \Rightarrow \quad \left|\varepsilon_{pct}\right| = \lambda\sqrt{\frac{3}{2(1+\nu_p)}} \text{ and } \left|\dot{\varepsilon}_{ps}\right| = \dot{\lambda}\frac{\sqrt{3}}{2} \Rightarrow \left|\varepsilon_{ps}\right| = \lambda\frac{\sqrt{3}}{2} \tag{40}$$

In this case the conversion of the tangent values that result from the table lookups is equally trivial:

$$\frac{\partial\sigma_s}{\partial\lambda} = \frac{\sqrt{3}}{2}\frac{\partial\sigma_s}{\partial\varepsilon_{ps}}, \quad \frac{\partial\sigma_t}{\partial\lambda} = \frac{\sqrt{3}}{\sqrt{2(1+\nu_p)}}\frac{\partial\sigma_t}{\partial\varepsilon_{pt}}, \quad \frac{\partial\sigma_c}{\partial\lambda} = \frac{\sqrt{3}}{\sqrt{2(1+\nu_p)}}\frac{\partial\sigma_c}{\partial\varepsilon_{pc}} \tag{41}$$

In the case of associated flow the conversion factors are not constants and must be evaluated at each time step

$$\frac{\partial\sigma_s}{\partial\lambda} \approx \frac{\partial\sigma_s}{\partial\varepsilon_{ps}}\frac{2\sigma_{vm}}{\|\mathrm{n}\|}\frac{\sqrt{3}}{2}, \frac{\partial\sigma_t}{\partial\lambda} \approx \frac{\partial\sigma_t}{\partial\varepsilon_{pt}}\frac{2\sigma_{vm}}{\|\mathrm{n}\|}\frac{3}{2(1+\nu_p)}, \frac{\partial\sigma_c}{\partial\lambda} \approx \frac{\partial\sigma_c}{\partial\varepsilon_{pc}}\frac{2\sigma_{vm}}{\|\mathrm{n}\|}\frac{3}{2(1+\nu_p)} \tag{42}$$

2.4. Rate effects

Plastics are usually highly rate dependent. A proper visco-plastic consideration of the rate effects is therefore important in the numerical treatment of the material law. Data to determine the rate dependency are based on uniaxial dynamic testing. If dynamic tests are available, then the load curve defining the yield stress in uniaxial tension is simply replaced by a table definition. Similar to MAT_24 this table contains multiple load curves corresponding to different values of the plastic strain rate. Subsequently table lookups involve determining static yield values for tension, compression and shear, as well as dynamic yield values in tension. Tangents with respect to the strain rate must also be evaluated:

$$\varepsilon_{ps} \Rightarrow \sigma_{s0}, \left.\frac{\partial \sigma_s}{\partial \varepsilon_{ps}}\right|_0, \varepsilon_{pt}, \dot{\varepsilon}_{pt} = 0 \Rightarrow \sigma_{t0}, \left.\frac{\partial \sigma_t}{\partial \varepsilon_{pt}}\right|_0, \varepsilon_{pt}, \dot{\varepsilon}_{pt} \Rightarrow \sigma_t, \frac{\partial \sigma_t}{\partial \varepsilon_{pt}}, \frac{\partial \sigma_t}{\partial \dot{\varepsilon}_{pt}}, \varepsilon_{pc} \Rightarrow \sigma_{c0}, \left.\frac{\partial \sigma_c}{\partial \varepsilon_{pc}}\right|_0$$

Furthermore it is assumed that the rate effect in compression and shear is similar to the rate effect in tensile loading: $\sigma_s = \sigma_{s0}\frac{\sigma_t}{\sigma_{t0}}, \quad \sigma_c = \sigma_{c0}\frac{\sigma_t}{\sigma_{t0}}$ .These tangents to the yield surface are computed consistently with the previous assumption leading to

$$\begin{aligned} &\frac{\partial \sigma_s}{\partial \varepsilon_{ps}} = \frac{\partial \sigma_s}{\partial \varepsilon_{ps}}\bigg|_0 \frac{\partial \sigma_{tc}}{\partial \varepsilon_{pt}}\left(\frac{\partial \sigma_{tc}}{\partial \varepsilon_{pt}}\bigg|_0\right)^{-1}, \quad \frac{\partial \sigma_c}{\partial \varepsilon_{pc}} = \frac{\partial \sigma_c}{\partial \varepsilon_{pc}}\bigg|_0 \frac{\partial \sigma_{tc}}{\partial \varepsilon_{pt}}\left(\frac{\partial \sigma_{tc}}{\partial \varepsilon_{pt}}\bigg|_0\right)^{-1} \\ &\frac{\partial \sigma_s}{\partial \dot{\varepsilon}_{ps}} = \frac{\partial \sigma_t}{\partial \dot{\varepsilon}_{pt}}\frac{\sigma_{s0}}{\sigma_{t0}}, \quad \frac{\partial \sigma_c}{\partial \dot{\varepsilon}_{pc}} = \frac{\partial \sigma_t}{\partial \dot{\varepsilon}_{pt}}\frac{\sigma_{c0}}{\sigma_{t0}} \end{aligned} \quad . \tag{43}$$

Although this approach is certainly questionable since rate effects may depend on the state of stress, it is justified by the fact that dynamic test results are not easily obtainable under shear and compression. A generalization involving table-type definitions for all three types of experiments could be implemented straight forward if needed.

2.5. Damage and failure

Numerous damage models can be found in the literature. Probably the simplest concept is elastic damage where the damage parameter (usually written as *d*) is a function of the elastic energy and effectively reduces the elastic moduli of the material. In the case of ductile damage, *d* is a function of plastic straining and affects the yield stress rather than the elastic moduli. This is equivalent to plastic softening. In more sophisticated damage models, *d* depends on both the plastic straining and the elastic energy (and maybe other factors) and affects yield stress as well as elastic moduli, see [13]. A simple damage model was added to the SAMP-1 material law where the damage parameter *d* is a function of plastic strain only. A load curve must be provided by the user giving *d* as a function of the (true) plastic strain under uniaxial tension. The value of the critical damage *Dc* leading to rupture is then the only other required additional input. The implemented damage model is isotropic. Furthermore the model uses the notion of the effective cross section, which is the true cross section of the material minus the cracks that have developed. We define the effective stress as the force divided by the effective cross section

$$\sigma = \frac{f}{A}, \quad \sigma_{eff} = \frac{f}{A_{eff}} = \frac{f}{A(1-d)} = \frac{\sigma}{1-d} \quad , \tag{44}$$

which allows to define an effective yield stress of $\sigma_{y,eff} = \frac{\sigma_y}{1-d}$, see [13]. By application of the principle of strain equivalence, stating that if the undamaged modulus is used, the effective stress corresponds to the same elastic strain as the true stress using the damaged modulus, one can write $E = \frac{\sigma_{eff}}{\varepsilon_e}, \quad E_d = \frac{\sigma}{\varepsilon_e} = E(1-d)$. Note that the plastic strains are therefore the same: $\varepsilon_p = \varepsilon - \frac{\sigma_{eff}}{E} = \varepsilon - \frac{\sigma}{E_d}$. No damage will occur under pure elastic deformation with this model. As an example we consider the case of a material that is perfectly plastic in its undamaged state.

Experimentally it can be seen that the damage parameter effectively reduces the elastic modulus. Consequently if unloading is performed at different strain values during the uniaxial tensile test, the different unloading slopes allow to estimate the damage parameter for a given plastic strain: $d(\varepsilon_{pt}) = 1 - \frac{E_d(\varepsilon_{pt})}{E}$. The damage model will thus be used essentially to fit the unloading behavior of the material. The two stage process of determining input data from a measured true stress/strain curve is illustrated below. In a first step the damage curve is derived as given in Figure 1.

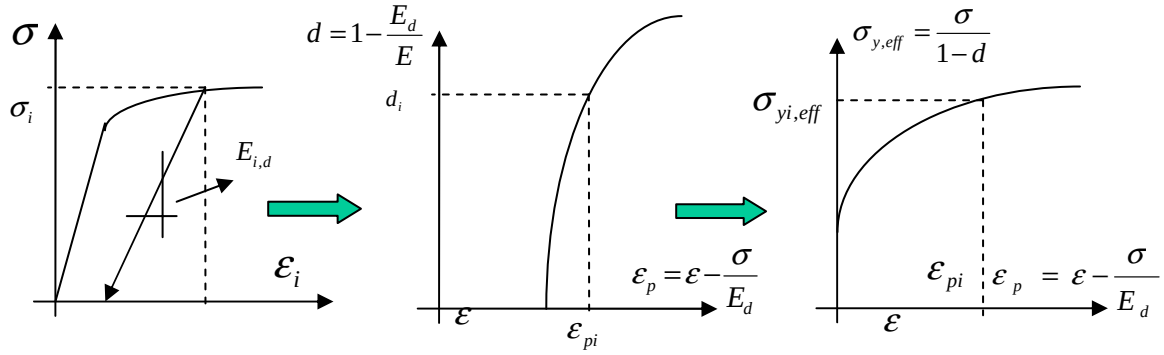

Figure 1: Determination of damage as a function of plastic strain

And in a second step the hardening curve is determined in terms of effective stresses. As usual the failure strain corresponds to the point where *d=0* and the rupture strain corresponds to the point where d reaches the critical value *Dc*. If the damage curve is given a negative identification number in the LS-DYNA input, then the hardening curve data are expected in terms of true stresses and the input preparation is performed as if there were no damage. In this case the numerically computed stress values will correspond to the input data and the damage model will seem to affect only the elastic moduli and thus the unloading/reloading behavior of the material.

2.6. Crazing

Many plastics and PP-EPDM in particular show a localized deformation process called crazing. The material will typically change colour and turn white in the craze. From a mechanical point of view crazing can be identified with a permanent increase of volume (volumetric plastic straining) and a low biaxial strength. To simulate crazing it may therefore be desirable to consider biaxial test data in the numerical model. In SAMP-1 the hardening curve resulting from a biaxial tensile test is therefore optional as input. The curve should give yield stress as a function of plastic strain and care must be taken to use the correct biaxial modulus when transforming from true strain to plastic strain. In many practical cases where biaxial data are available, some other test result will be missing. In these cases the missing data are generated internally from the biaxial test result assuming a quadratic isotropic yield surface and the material law formulation is not changed.

2.7. Numerical implementation

Rate-independent plasticity iterations

To solve the equations of elasto-plasticity, the explicit cutting plane algorithm was selected. A complete review of the implementation is given below and is based on works of [11]. Consider the following set of equations defining the SAMP-1 material law:

$$\begin{aligned}
&\dot{\sigma} = 2G\left(\dot{\varepsilon}_d - \dot{\varepsilon}_d^p\right) + K\left(\dot{\varepsilon}_v - \dot{\varepsilon}_v^p\right)\delta && \textit{material law}\\
&\dot{q} = \begin{pmatrix} \dot{A}_0 \\ \dot{A}_1 \\ \dot{A}_2 \\ \dot{\alpha} \end{pmatrix} = \dot{\lambda} h = \dot{\lambda} \begin{pmatrix} \partial A_0 / \partial \lambda \\ \partial A_1 / \partial \lambda \\ \partial A_2 / \partial \lambda \\ \partial \alpha / \partial \lambda \end{pmatrix} && \textit{hardening rule}\\
&\dot{\varepsilon}^p = \dot{\lambda} r = \dot{\lambda}\frac{\partial g}{\partial \sigma} && \textit{flow rule}\\
&f = \begin{cases} \sigma_{vm}^2 - A_0 - A_1 p - A_2 p^2 \le 0 & iquad = 1 \\ \sigma_{vm} - A_0 - A_1 p - A_2 p^2 \le 0 & iquad = 0 \end{cases} && \textit{yield surface}
\end{aligned} \tag{45}$$

Here we can further specify the flow rule as follows:

$$\begin{aligned}
&\left.\begin{matrix} iquad = 0/1 \\ \alpha \ge 0 \end{matrix}\right\} \Rightarrow \dot{\varepsilon}^p = \dot{\lambda} r = \dot{\lambda}\frac{\partial g}{\partial \sigma} = \dot{\lambda}\frac{9s - 2\alpha p\delta}{6\sqrt{\sigma_{vm}^2 + \alpha p^2}}\\
&\left.\begin{matrix} iquad = 1 \\ \alpha > 0 \end{matrix}\right\} \Rightarrow \dot{\varepsilon}^p = \dot{\lambda} r = \dot{\lambda}\frac{\partial g}{\partial \sigma} = \dot{\lambda}\frac{9s + (A_1 + A_2 p)\delta}{\sqrt{6\sigma_{vm}^2 + \frac{(A_1 + A_2 p)^2}{3}}}
\end{aligned} \tag{46}$$

It should be noted that no associated flow has been implemented for the alternative yield condition (*iquad=0*).

The damage model

The implementation of the damage model is trivially simple since the entire plasticity algorithm is performed in terms of effective stresses without any modification. In case the damage load curve has a negative identification number, the algorithm just amounts to modify the elastic modulus in each iteration:

$$E_{d,n}^k = E\left(1 - d_n^k\left(\varepsilon_{pt,n}^k\right)\right) \tag{47}$$

Rate effects

A constitutive law for visco-plastic materials is given for instance in [12] as:

$$\dot{\lambda} = \frac{\langle \Phi(f) \rangle}{\tau} \tag{48}$$

Here *f* is the yield function, so in our case $f = \sigma_{vm}^2 - A_0 - A_1 p - A_2 p^2$. The Föppl symbol (also known as McCauley-brackets) is used to indicate that the (visco-)plastic strain rates are zero as long as the state of stress is elastic. It should be emphasized at this point that the coefficients of the yield function *f* are not rate dependent. Φ must be a dimensionless function and τ is a relaxation time. In general Φ need not be dimensionless and the visco-plastic constitutive law is given as

$$\dot{\boldsymbol{\varepsilon}}_{\boldsymbol{p}} = \frac{\langle \Phi(f) \rangle}{2\eta} \boldsymbol{r} \Rightarrow \dot{\lambda} = \frac{\langle \Phi(f) \rangle}{2\eta} . \tag{49}$$

Here η has the dimension of a viscosity if Φ has the dimension of a stress. This formulation is typically based on a constant viscosity and either a power law or exponential expression for Φ and seems usually sufficient to describe the rate dependency of metals.
In the case of plastics, the rate dependency of the material is more pronounced and potentially has a different character. Therefore a tabulated formulation was chosen which gives the user full flexibility for fitting the model to test data. Uniaxial dynamic tensile tests allow tabulating the dynamic stress as a function of plastic strain and plastic strain rate. In the visco-plastic regime

$$2\eta\dot{\lambda} = \Phi(f) \Rightarrow f = \Phi^{-1}(2\eta\dot{\lambda}) \tag{50}$$

is obtained. Furthermore the constitutive equation is solved by $f(\lambda) - \Phi^{-1}(\dot{\lambda}) = 0$. This shows that the viscous overstress expressed by a positive value of the yield function *f* can be identified with the inverse function of Φ. In contrast to the rate independent case now the constitutive law instead of the consistency equation is enforced. The cutting plane algorithm is applied accordingly.

3. Applications

3.1. Yield surfaces of different thermoplastics

As a first example, the application of the present model due to prediction of yield for different thermoplastics is shown. For a review of methods commonly used in crash simulation, see [7], [8]. The results obtained by SAMP-1 are compared to the von Mises yield criterion. It must be emphasized that this criterion is usually used in crash simulation for modeling of thermoplastics. For a better understanding, the curves given in Figure 2 to Figure 4 are plotted in both the plane stress plane and the invariant plane. The experimental results are taken from Bardenheier [5].

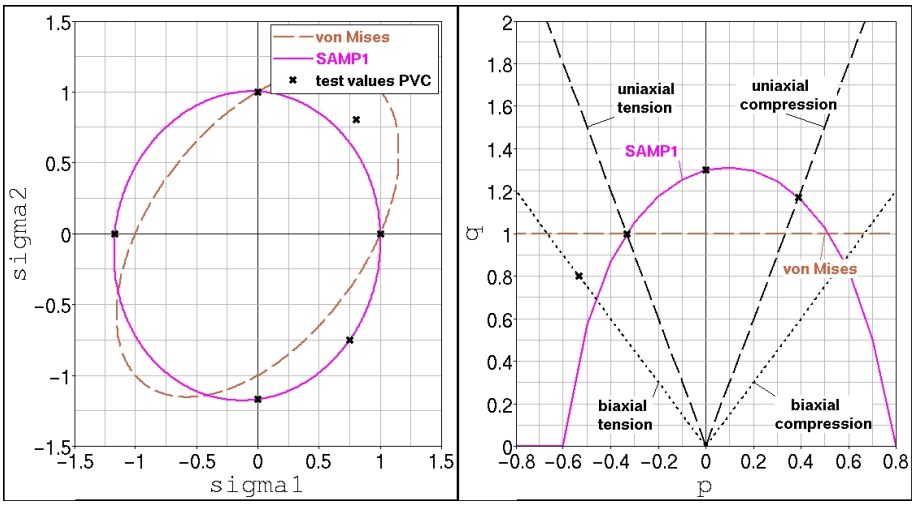

Figure 2: Yield surface of polyvinyl chloride (PVC)

In Figure 2, test data of polyvinyl chloride (PVC) is depicted. The dotted line represents results of the von Mises yield criterion and the solid line represents results obtained by SAMP-1. As can be seen, the von Mises yield surface is not capable to consider the different behavior in compression, tension and shear. SAMP-1 yields to a much better agreement with the test. However, the experimental result under biaxial tension is not fitted exactly but approximated sufficiently. A method for further improvement of the result under biaxial tension is given by the least square fit which will be explained subsequently.

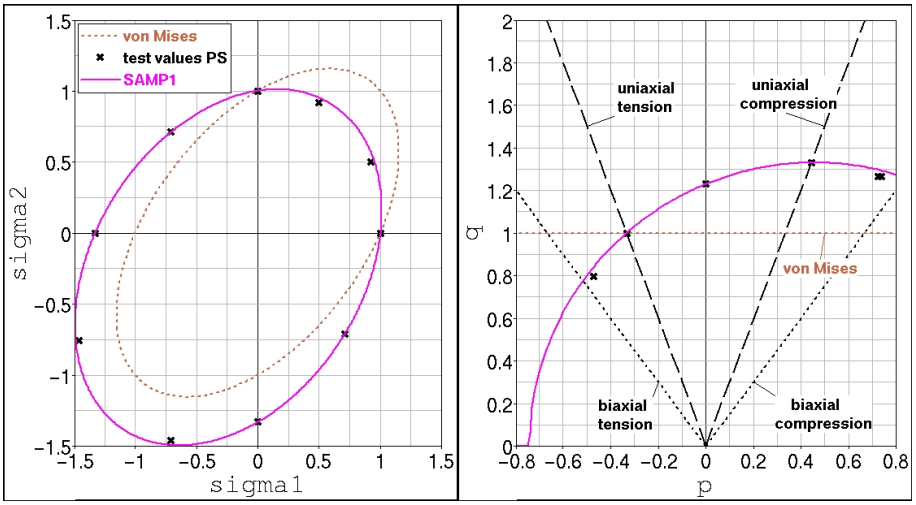

Figure 3: Yield surface of polystyrene (PS)

As a next example for a polymer that is widely used in engineering practice, polystyrene (PS) is regarded. For this polymeric material, more experimental results under different loading directions are available, see
Figure 3. Again, the von Mises criterion cannot describe the challenging material response. The results obtained by SAMP-1 are in good agreement with the experimental findings. This identifies the present model as an appropriate material law for polymers. Similar results can be observed for a polycarbonate (PC). Note that for polystyrene a convex yield surface is obtained in

the p-q-plane. Three distinct points of the yield surface can be used directly to define the quadratic yield function in SAMP-1. In order to take four samples into account for the quadratic yield criterion, a least square approximation is applied. By such a numerical treatment, the experimental data under biaxial tension as well as test data of tension, compression and shear loading can be considered simultaneously.
In Figure 4, an acrylonitrile butadiene styrene (ABS) shows noticeable agreement. In the yield surface, this results in a softening behavior under biaxial tension. As can be seen, using compression, tension and shear only, the yield behavior cannot be described sufficiently by the SAMP-1 criterion. If biaxial tension is considered additionally by a least square fit, the (still convex) yield surface is much closer to the experimental data.

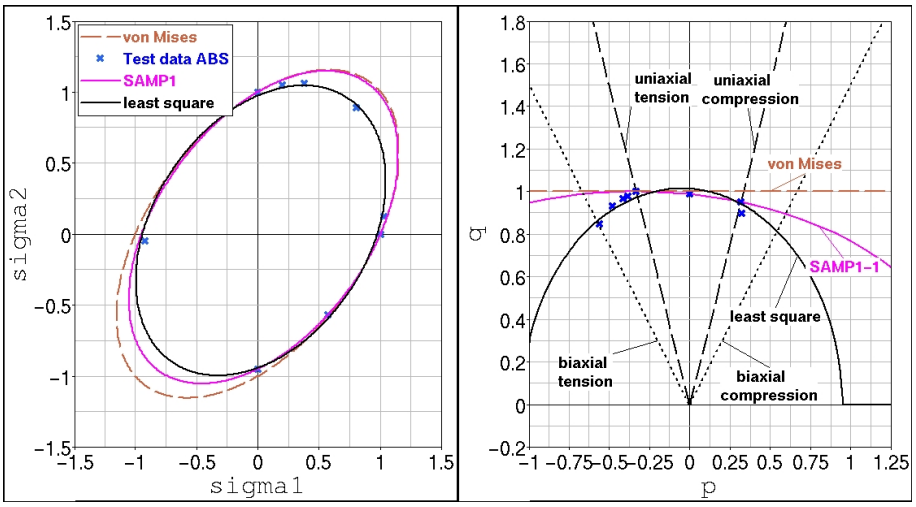

Figure 4: Yield surface of acrylonitrile butadiene styrene (ABS)

3.2. Verification and validation of PP-EPDM

3.2.1. Dynamic tensile tests

The strain rate dependency of SAMP-1 is investigated by the simulation of dynamic tensile tests. The experimental setup consists of a bone shaped specimen with a total length of 48.6mm, see Figure 5. The area of uniaxial stress (8x20mm) is highlighted in the picture.

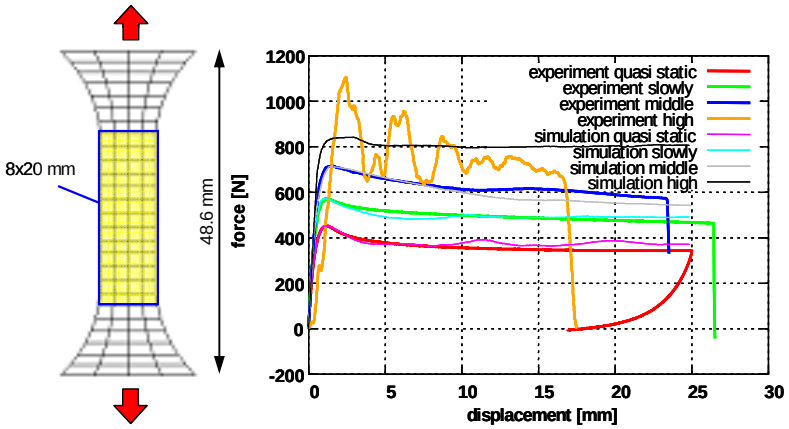

Figure 5: Dynamic tensile tests at different strain rates

The test data is input in the material card by defining tabulated local stress-strain curves measured at different strain rate levels. The bone shaped specimen is discretized with an element size that is typically used in crash simulation. The choice of the same element size is necessary because of the well known strong mesh dependency due to strain-softening. The global force and displacement are compared to the experimental response. The results are given in Figure 5. At this point, it has to be emphasized again that in SAMP-1 a real visco-plastic formulation is implemented, i.e. relaxation effects are taken into account as it is known from MAT_PIECEWISE_LINEAR_PLASTICITY with VP=1.

3.2.2. Quasi-static tensile tests with unloading

In the numerical simulation of thermoplastics, the prediction of the elastic rebound of structures is an important issue, especially for pedestrian protection. The unloading behavior is dominated by visco-elastic effects, i.e. viscosity below permanent deformation. However, visco-elasticity is not considered within SAMP-1 so far. Nevertheless, unloading can be approximated linearly by elastic damage, see [7], and [8] for details. For parameter identification, unloading tests at different strain levels were performed. The unloading path can then be approximated by the damage parameter $d = d(\varepsilon_p)$ which acts on the effective Young's modulus.

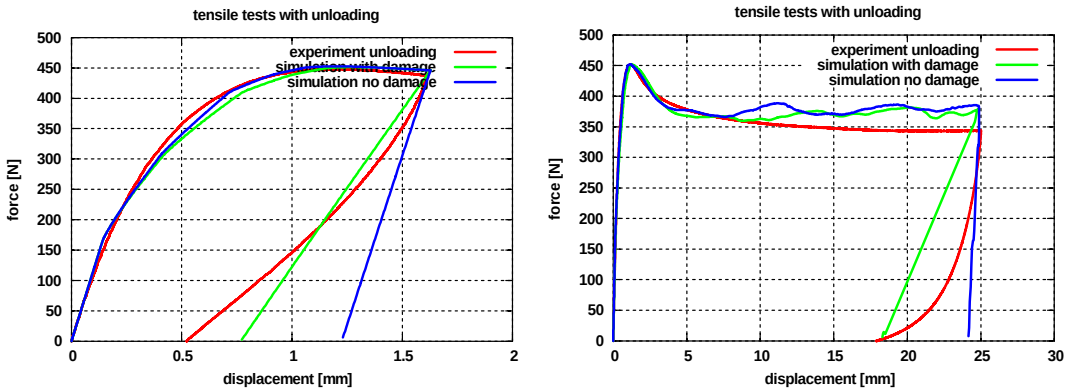

Figure 6: Tensile tests with unloading at different strain levels

In SAMP-1, this damage function can be tabulated in a load curve. Since the damage model of [13] is used, the yield function $\sigma_y(\varepsilon_p)$ is affected by damage, too. That is, softening of the stress-strain curve may be expected. Usually, if elastic damage is to be taken into account only, the yield stress has to be modified according to $\sigma_y \mapsto \sigma_y/(1-d)$ as it is known from MAT_PLASTICITY_WITH_DAMAGE. To avoid such a cumbersome procedure, an additional feature has been implemented. If LCID-d is negative in the input, the modification of the yield stress is realized internally and the original stress-strain curve is reflected. The simulation results of a simple tensile test in comparison with experimental results are depicted in Figure 6. As can be seen, the reduction of the elastic parameters for increasing plastic strains considers the unloading behavior approximately and the experimental stress-strain curve is recovered.

3.2.3. Compression test

The different behavior of thermoplastics in compression and tension does not comply with a von Mises type of plasticity as it is used in MAT_PIECEWISE_LINEAR_PLASTICITY. In SAMP-1, the direct input of experimental data obtained from compression tests allows a straight forward treatment of the problem. In Figure 7, a draft of the experimental setup consisting of a bone shape specimen with a total length of 176.33mm is given. The area (40x60mm) of uniaxial stress is highlighted and, additionally, the dog bone specimen is supported perpendicular to the drawing plane to avoid local buckling. The specimen is again discretized with an element size used in full car models and the material properties are validated subsequently. The global force and displacement are compared to the measured response. The results given in Figure 7 show a good agreement. Note that the local stress-strain curve obtained in the experiment is simply used in the material card for the LCID-c. However, a pure uniaxial stress state is hard to achieve in both experiment and simulation. A certain interaction with tension and shear cannot be avoided completely. This is even more pronounced in the shear test of the next example.

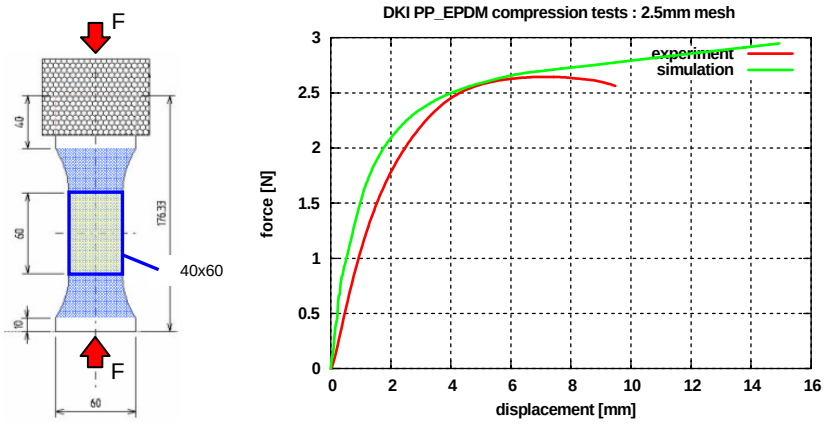

Figure 7: Compression test

3.2.4. Shear test

In Figure 8, a shear test has been simulated by using SAMP-1. Although a pure shear stress is certainly not given, the test can be simulated at least up to yield in a satisfactory way. For larger displacements, the model acts too stiff due to the large element size. Clearly, a further refinement is not advisable with regard to the time step size in a full car model. The effect is getting less pronounced for a finer mesh, though.

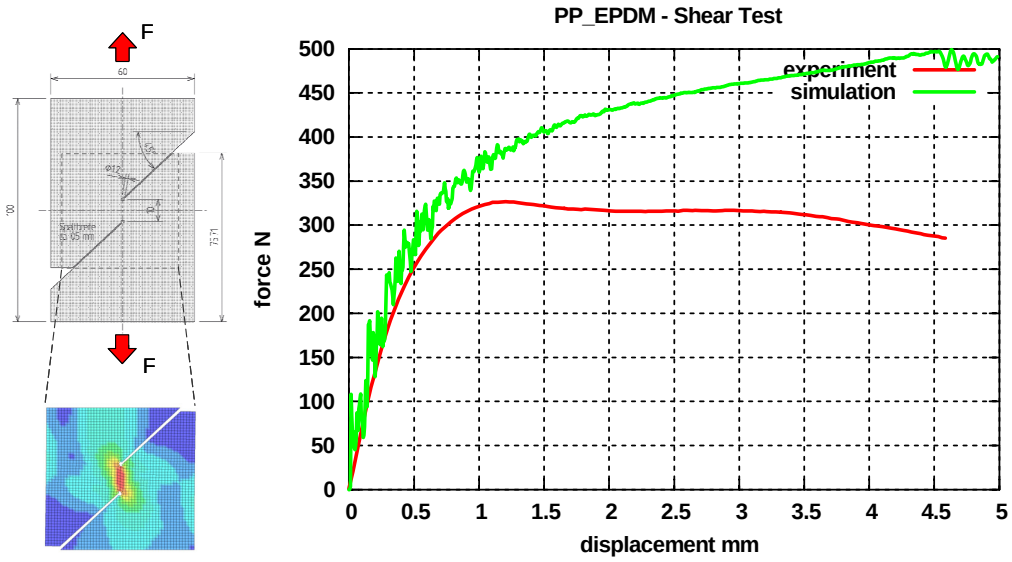

Figure 8: Shear test

3.2.5. Bending test

In Figure 9, the reaction force versus the displacement of a quasi-static three point bending test is shown. Because of the higher yield stress under compression, it is not possible to simulate the bending test by using a von Mises criterion solely based on the tensile test data. With SAMP-1, where the higher yield stress taken from the experiment under compression is considered, the bending test can be simulated with good agreement.

In conclusion it can be said that all the effects associated with thermoplastics given in the examples can be approximately considered in the present material model: necking and strain rate effects by visco-plasticity, unloading behavior by a (1-d)-damage model, different behavior under compression and tension and thus a correct bending stiffness by the chosen yield surface.

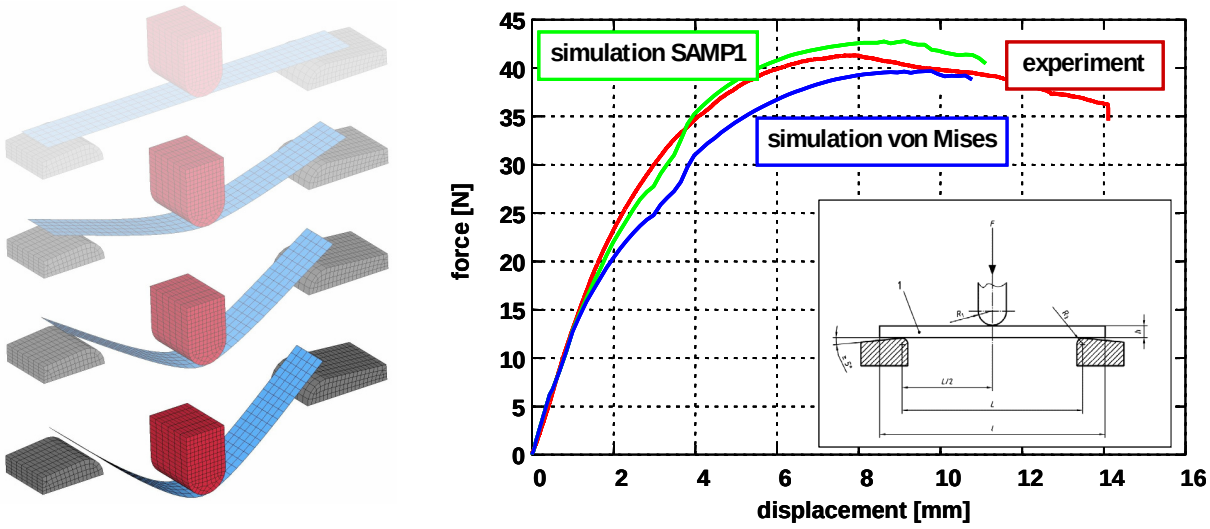

Figure 9: Three-point-bending test

4. Conclusion and Outlook

Balancing the need for accuracy and respect for the actual physics with easiness of use, robustness and efficiency, we have chosen a theoretical and numerical framework that is familiar, yet reasonably general. For many plastics we are able to obtain a reasonable fit of the experimental data; even if its rate dependency is high. The material law is equipped with special-purpose options to obtain a numerically robust response. The tabulated input will be transparent to most users. However, the application is limited to ductile plastics that are initially isotropic and remain isotropic throughout the deformation process. In many cases the test data is hard to fit with a quadratic yield surface or will lead to a concave yield surface. Moreover, non-convex yield surfaces potentially generate problems in the numerical algorithm since a unique solution is no longer guaranteed.

Future work will focus on the load-induced anisotropy which develops naturally in plastics and on the implementation of more advanced damage and failure models. On the somewhat longer term, a visco-elasto-visco-plastic approach is envisioned to accommodate rate effects in the elastic region. Combined with the anisotropic formulation this can result in a model suitable also for fiber reinforced components. Furthermore, the model is not restricted to thermoplastics, it should be emphasized that the model is also capable to describe the behavior of structural foams and adhesives at least phenomenologically. Moreover, metallic materials like steels and aluminum are included as special cases exhibiting zero volumetric plastic strain.

5. Literature

[1] LS-DYNA, Theoretical Manual / User Manual, Livermore Software Technology Corporation.

[2] P.A. Du Bois: Crashworthiness Engineering Course Notes, Livermore Software Technology Corporation, 2004.

[3] S. Kolling, A. Haufe: A constitutive model for thermoplastic materials subjected to high strain rates, Proceedings in Applied Mathematics and Mechanics • PAMM 5: 303-304.

[4] T. Frank, A. Kurz, M. Pitzer, M. Soellner: Development and validation of numerical pedestrian impactor models. 4th European LS-DYNA Users Conference, pp. C-II-01/18, 2003.

[5] R. Bardenheier: Mechanisches Versagen von Polymerwerkstoffen. Hanser-Verlag, 1982.

[6] D.C. Drucker, W. Prager: Soil mechanics and plastic analysis or limit design. Quaterly of Applied Mathematics, 10:157-165, 1952.

[7] P. A. Du Bois, S. Kolling, M. Koesters, T. Frank: Material behavior of polymers under impact loading. International Journal of Impact Engineering 32 (2006) 725-740.

[8] P.A. Du Bois, M. Koesters, T. Frank, S. Kolling: Crashworthiness analysis of structures made from polymers. 3rd LS-DYNA Forum, Bamberg, Germany 2004. Conference Proceedings, ISBN 3-9809901-0-9, pp. C-I-01/12.

[9] A. Haufe, P.A. Du Bois, S. Kolling, M. Feucht: A semi-analytical model for polymers subjected to high strain rates. 5th European LS-DYNA Users' Conference, Birmingham, England, 2005, Conference Proceedings, ARUP UK, pp. 2b-58.

[10] A. Haufe, P.A. Du Bois, S. Kolling, M. Feucht: On the development, verification and validation of a semi-analytical model for polymers subjected to dynamic loading. International Conference on Adaptive Modeling and Simulation, ADMOS, Barcelona, Spain, 2005, Conference Proceedings.

[11] J.C. Simo, T.J.-R. Hughes: Elastoplasticity and viscoplasticity – computational aspects. Springer Series in Applied Mathematics, Springer, Berlin, 1989.

[12] T.J.-R. Hughes: Efficient and simple algorithms for the integration of general classes of inelastic constitutive equations including damage and rate effects. In T.J.-R. Hughes ,T. Belytschko: nonlinear finite element analysis course notes, 2003.

[13] J. Lemaitre, J.-L. Chaboche: Mécanique des matériaux solides, Dunod, 1988.

[14] W.W. Feng, W.H. Yang: general and specific quadratic yield functions, composites technology review.

[15] S. Kolling , A. Haufe, M. Feucht, P.A. Du Bois: A semianalytical model for the simulation of polymers. 4th LS-DYNA Forum, Germany 2005, Conference Proceedings, ISBN 3-9809901-1-7, pp. A-II-27/52.